ISSN 2321-807X
Volume 12 Number12
Journal of Advances in chemistry

Synthesis, structural and optical properties of Mn doped ZnO nanoparticles and their antibacterial application

A.Srithar[1], J.C.Kannan[2], T.S.Senthil[3]
[1]Department of Physics, The Kavery College of Engineering, Salem, Tamilnadu - 636 453, India.
mrsriphy@gmail.com
[2]Department of Physics, KSR Institute of Engineering and Technology, Tiruchengode – 637215.
vasikanna@gmail.com
[3]Department of Physics, Erode Sengunthar Engineering College, Erode - 638 057, India.
tssenthi@gmail.com

ABSTRACT

In the present investigation, $Mn_xZn_{1-x}O$ (x = 0.05, 0.075 and 0.1%) nanoparticles have been synthesized by simple precipitation method. Their structural, morphological and optical properties were examined by using X-ray diffraction (XRD), Field emission scanning electron microscopy (FESEM), Energy dispersive X-ray spectroscopy (EDX), High resolution transmission electron microscopy (HRTEM), Fourier transform infrared spectroscopy (FTIR), Raman spectroscopy, Differential scanning calorimetry (DSC) and UV-Visible spectroscopy. The Powder X-ray diffraction studies confirmed that the manganese doped ZnO have a single phase nature with hexagonal wurtzite structure and Mn successfully incorporated into the lattice position of Zn in ZnO lattice. The FESEM and HRTEM images are coincided with each other for aggregation of particles in nature. The elemental analysis of doped samples has been evaluated by EDX. The antibacterial activity of Mn doped ZnO nanoparticles has also been examined.

Keywords

ZnO, Precipitation method, Nanoparticles, Band gap, Antibacterial activity.

Academic Discipline And Sub-Disciplines

Physics

SUBJECT CLASSIFICATION

Nano technology

TYPE (METHOD/APPROACH)

Precipitation method.

1. INTRODUCTION

In recent years, large number of investigations has focused on transitional metals such as La, Fe, Pd and Mn doped ZnO nanoparticles, due to its direct band gap of 3.37 eV at room temperature with large excitation binding energy of 60 meV [1]. Compared with all other metal oxides, it is abundant in nature and eco - friendly. These characteristics make this material attractive for many applications such as solar cells, optical coatings, photocatalysts, antibacterial activities, electrical devices, active medium in UV semiconductor lasers and gas sensors [2]. Hence, it has influenced the attention of researchers and scientists to develop ZnO in the field of science and technology.

Compared with pure ZnO nanoparticles, transition metal doped ZnO nanoparticles enhances the visible light absorption by generating energy states within the band gap, which act as intermediate steps for electrons in their transitions between the valence and conduction bands due to photoexcitation [3-5].Doping of 3d transition metal Mn into the ZnO lattice tailors the various properties of ZnO. Further, it has been reported that Mn doping with an optimal concentration narrows the band gap of ZnO thus extending the absorption into the visible light region [6]. ZnO nanoparticles uniformly doped with Mn have advantages as dilute ferromagnetic semiconductor with characteristic luminescence [7].

Now-a-days microbial contamination is a serious issue in healthcare and food industry, so that the development of antimicrobial agents and surface coatings has been attracting and increasing attention in recent years. It has been recognized that toxicity of nanoparticles are generally high. Therefore, developments of nanoparticles with antimicrobial properties are of considerable interest [2].

Mn doped ZnO nanoparticles have been synthesized in several forms (Thin film, bulk and nanoparticles) by RF sputtering, Pulsed laser deposition (PLD), Chemical vapour deposition (CVD) and simple sol–gel method [8-12]. They, herein report the synthesis of different concentration of Mn doped ZnO nanoparticles by precipitation method. The characterization of $Mn_xZn_{1-x}O$ (x = 0.05, 0.075 and 0.1%) nanoparticles were accomplished by X-ray diffraction, Scanning electron microscopy (SEM), Transmission electron microscopy (TEM), Energy dispersive X-ray spectroscopy (EDX), Fourier transform infrared spectroscopy (FTIR), Raman spectroscopy, Differential scanning calorimetry (DSC) and UV-Visible absorbance spectroscopy methods. The antibacterial activity of the various concentrated (0.05, 0.075 and 0.1%) Mn doped ZnO nanoparticles have also been examined.

2. EXPERIMENTAL

2.1. Physical measurements

The synthesized samples were recorded using powder X-ray diffractometer XPERT PRO X-RAY with the CuKα radiation source (λ=1.5406 nm). The morphology of the samples was recorded using Scanning electron microscopeJSM-6701F-6701 and particle size was recorded using transmission electron microscope TECNAI G2 Model. The elemental analysis was carried out by using energy dispersive X-ray spectroscopy (EDX).The composition quality of the synthesized material is characterized by Fourier transform infrared Thermo Nicolet 6700 FT-IR spectrophotometer in the range of 400 to 4000 cm^{-1}.The Raman spectra have been recorded with a JASCO NRS 3300 spectrophotometer. Differential scanning calorimetry (DSC) performed using thermal analysis system DSC Q20 V24.10 Build 122, and studies the phase variations during crystallization. The absorbance spectra have been recorded in UV-visible spectrometer JASCO V-670. The *in vitro* antibacterial screening against *Staphylococcus aureus* and *Escherichia coli* for the nanoparticles have been carried out by agar disc diffusion method.

2.2. Preparation of Mn doped ZnO

ZnO nanoparticles have been prepared using the required precursors by precipitation method. An aqueous solution of 0.3M zinc acetate dihydrate $\{Zn[CH_3(COO)]_2 2H_2O\}$ is dissolved in 50 ml distilled water and stirred for about 30 minutes at room temperature. After the reaction time, add drop by drop 50ml of 0.75Msodium hydroxide (NaOH) solution. The solution mixture was stirred for 4 hours at room temperature. After 4 hours the deposited precipitate is centrifuged and washed with distilled water and ethanol several times. The samples are then suspended in ethanol and allowed to age for 2 hours without stirring. After centrifugation, the samples then dried in oven at 70°C for 2 hours. Then, the prepared ZnO nanoparticles are placed in the middle of muffle furnace in silica crucible. The samples have been annealed at 450°C for an hour.

Similarly for Mn doping, the required amount of manganese nitrate (x = 0.05, 0.075 and 0.1 %) was added into the zinc acetate dihydrate with 100 ml water and stirred for about 30 minutes at room temperature. In that solution, 50 ml of 0.75 mole sodium hydroxide solution was added drop wise, the obtained solution is aged, centrifuged and annealed in a similar way as mentioned above.

2.3. Determination of antibacterial activity

The antibacterial activities of the prepared samples were evaluated using agar disc diffusion method. The microorganisms used for this study were Staphylococcus aureus and Escherichia coli. 7 mm filter paper discs were impregnated with 20 mL of each of the different dilutions. The discs were allowed to remain at room temperature until complete diluents evaporation and kept under refrigeration until ready to be used. Discs loaded with samples were placed onto the surface of the agar. Then, the diameters of the inhibition zones were determined in millimeters.

3. RESULTS AND DISCUSSION

3.1. XRD analysis

The phase formation of $Mn_xZn_{1-x}O$ is confirmed by X-ray powder diffraction spectroscopy (Fig.1a). The pattern shows strong and sharp peaks, which confirm the hexagonal wurtzite structure of ZnO. Interestingly, the XRD pattern of Mn doped samples show no much change when compared with the pattern of un-doped sample, which confirms that there is no additional phase formation but there is a small shift to larger angle compared to pure ZnO diffraction pattern. For Mn doping the average crystallite size increases as 18, 25 and 26 nm for 0.05, 0.075 and 0.1 % Mn doped ZnO nanoparticles respectively.

The average crystallite size are calculated using the Scherrer's formula,

$$d = \frac{0.9\,\lambda}{\beta Cos\theta}$$

Where d is the average crystalline size, λ is the wavelength of radiation used; θ is the Bragg angle and β is the full width at half maxima (FWHM).

When doping concentration increases, the dopants enhance the agglomeration of particles and hence crystallite size increases. The increase in crystallite size subsequently reduces the band gap, which causes the red shift of absorption band [13]. The diffraction peaks at 2θ (degree) of 31.91, 34.50, 36.33, 47.64, 56.71, 63.01, 68.01 and 69.25 are respectively indexed to (100), (002), (101), (102), (110), (103), (112) and (201) planes of ZnO. They are in good accordance with the JCPDS card No. 75-0576.

The high intensity peaks such as (100), (002) and (101) showed in Fig. 1b indicates that the preferential orientation for the nanoparticle along the c-axis. There is no trace of manganese related phase was detected up to 0.075% of Mn doped ZnO nanoparticles. This indicated that the Mn ions substituted Zn sites without changing the crystal structure of ZnO without

ISSN 2321-807X
Volume 12 Number12
Journal of Advances in chemistry

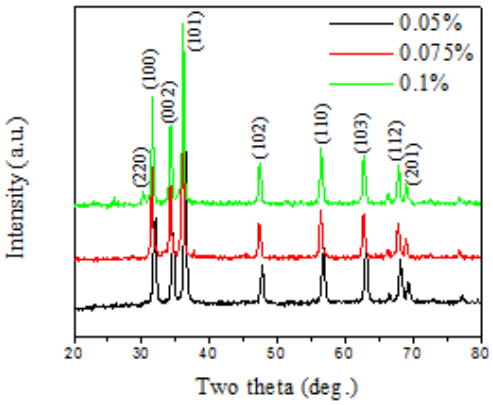

Fig 1a: XRD patterns of Mn doped (0.05, 0.075 and 0.1%) ZnO nanoparticles

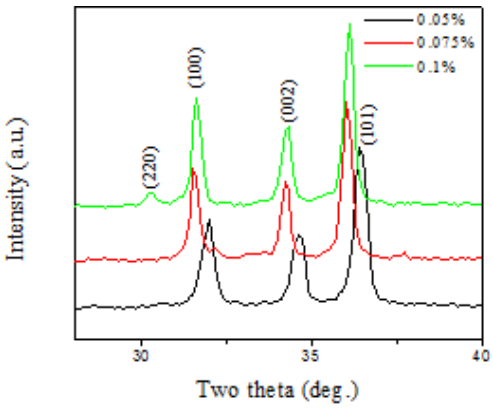

Fig 1b: Shifting of XRD peaks to higher degrees with increasing of Mn concentration

any precipitated phase or clustering. However with 0.1% of Mn doping, the appearance of an additional peak at 30.24^{o} may assigned to Mn_3O_4. That is to say, not all the stoichiometric Mn^{2+} has entered the ZnO lattice, the rest of Mn^{2+} has been oxidized into manganese oxide [14]. The incorporation of Mn^{2+} into ZnO lattice is evidenced by the shrinkage or the expansion of the lattice parameters of ZnO in response to the transition metal dopant up to 0.075% Mn after which both a and c parameter show increase. This increase is accounted for the fact that ionic radius of Zn^{2+} (0.74Å) is smaller than that of Mn^{2+} (0.83 Å). Such change in lattice parameters is indicative of the incorporation of Mn ions inside the ZnO lattice [7].

3.2. Field emission scanning electron microscopy

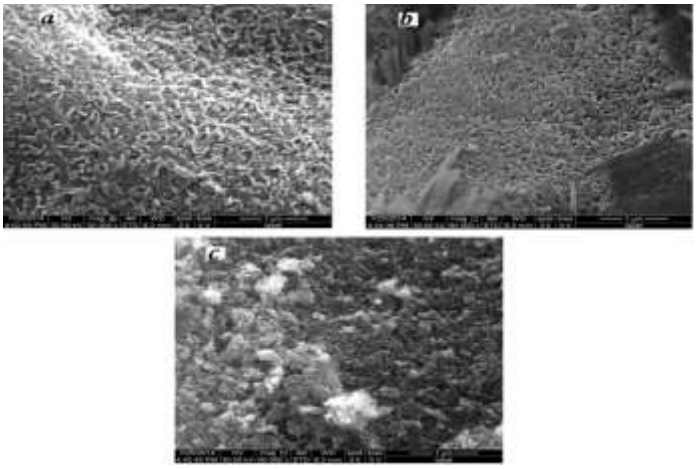

Fig 2: FESEM images of (a) 0.05% (b) 0.075% (c) 0.1% Mn doped ZnO nanoparticles

The surface morphological properties of the nanoparticles were analyzed by using FESEM (Fig.2) pattern of different concentrations of Mn doped ZnO nanoparticles. The amount and kind of dopant plays an important role on the surface properties and it is clearly identified from FESEM patterns [15]. At lower concentration, the $Mn_xZn_{1-x}O$ nanoparticles are merged and appear as rice like grains. When the doping concentration increases, well-formed nanoparticles are appeared on the surface with nanorod like structures. Whereas in the case of 0.1% Mn doped ZnO, the morphology of particles significantly changes from rods to merging like granules [16]. The incorporated Mn in Zn lattice sites, changes the nanorod morphology to bound grains. The small particles are agglomerated and bound one another to form spherical shape of Mn doped ZnO nanoparticles due to the increase of doping concentration.

3.3. Energy dispersive X-ray spectroscopy

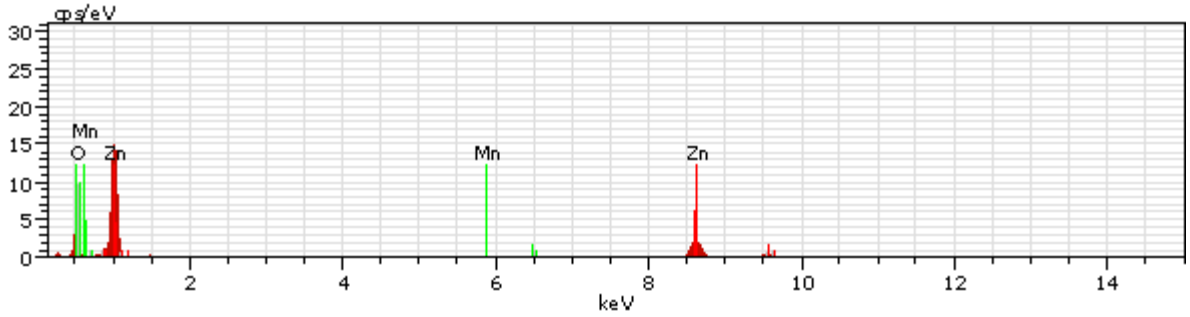

Fig 3: EDX analysis of$Mn_xZn_{1-x}O$ (x= 0.1%) nanoparticles

The Energy dispersive X-ray spectroscopy of the Mn doped ZnO nanoparticles was recorded to confirm the presence of Mn, Zn and O (Fig.3). The spectra showed that the atomic ratio of Zn, Mn and O is 8.60:0.32:91.08.This confirms the presence of Mn in the ZnO particles with wt% less than the nominal values of Mn in ZnO. Manganese is different from other transition metals when substituted in an $A^{II}B^{VI}$ matrix, since it forms stable phases over a wide range of compositions. It appears that the ease with which manganese substitutes for the group II elements in the zinc blende and wurtzite structures results from the fact that the 3d orbitals of Mn are exactly half filled [14].

3.4. High resolution transmission electron microscopy

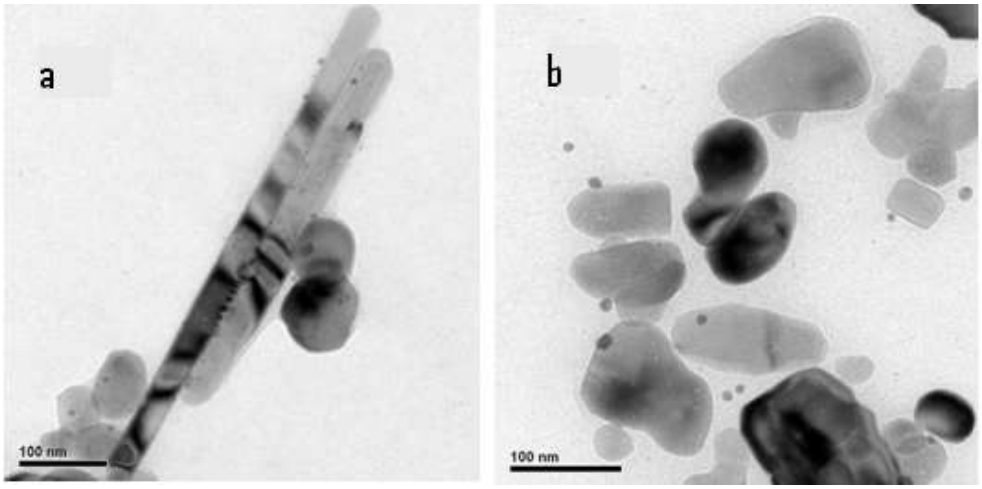

Fig 4: HRTEM images of (A) 0.075% (B) 0.1% Mn doped ZnO nanoparticles

The high resolution transmission electron microscope (HRTEM) image reveals that the size and morphology of Mn doped ZnO nanoparticles. Figure 4a (0.075%) shows the composed of polyhedral particles, which have a slight tendency to aggregate as nanorods [17]. Figure 4 (b) shows 0.1% Mn doped ZnO nanoparticles and the average size of the particle is found to be approximately 23.52 nm, which is in good agreement with the XRD results.

3.5. Fourier transform infrared spectroscopy

FTIR spectral data gives the information about functional groups present in a system, the molecular geometry, inter and intra molecular interactions. The FTIR spectra of the synthesized $Mn_xZn_{1-x}O$ (x = 0.1%) nanoparticles shown in figure 5. The peak at 611 cm^{-1} is assigned to Mn - O bending [18]. The peak appeared around 3479 cm^{-1} is assigned to O - H stretching vibration of H_2O in Zn - O lattice. The peak around 1619 cm^{-1} is assigned to H – O – H bending vibration, due to the presence of small amount of H_2O in ZnO nanoparticles.

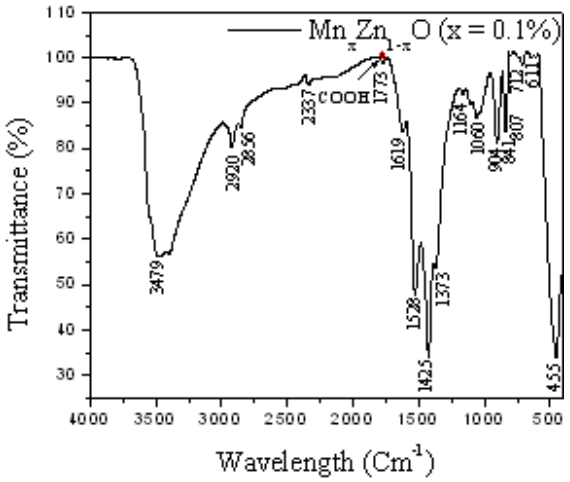

Fig 5: FTIR spectrum of $Mn_xZn_{1-x}O$ nanoparticles

The peak around 2337 cm^{-1} is the existence of CO_2 molecule in air [19]. Peaks observed in the range from 1200 to 1600 cm^{-1} can be attributed to the stretching vibration of C = O (asymmetric stretching). The peaks at 2856 and 2920 cm^{-1} are due to C-H bond bending and stretching mode [20].The above FTIR spectra showed that the C = O and C - O stretching vibration bands of COOH are around 1773 and 1060 cm^{-1} [21,22]. A peak with low intensity at 712 cm^{-1} can be assigned to the ZnO stretching mode [23]. The peak at 841cm^{-1} is appeared due to C – O – C – O bonds [22]. The strong peak appeared around 455 cm^{-1} is due to Zn – O stretching vibration [24]. The absorption peak at 807 cm^{-1} is due to the formation of tetrahedral coordination of Zn. The peak around 1164cm^{-1} indicates that the saccharide structure of ZnO nanoparticles [25]. The peak at 904 cm^{-1} is due to C – O – C vibrations [26].

3.6. Raman spectroscopy

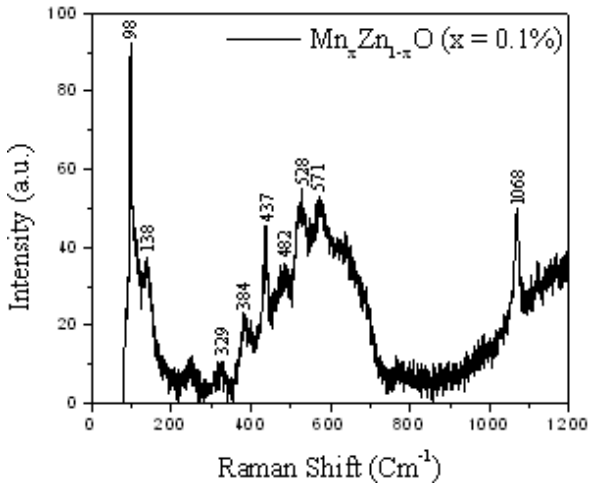

Fig 6: Raman Spectrum of $Mn_xZn_{1-x}O$ nanoparticles

Raman spectroscopy used to identify the crystal quality, structural defects and disorder formation of the sample. Fig. 6 clearly showed that the prepared sample consists of nine peaks located at about 98, 138, 329, 384, 437, 482, 528, 571 and 1068 cm^{-1}. In this peaks, 98, 138 and 384 $cm^{-1}$are the fundamental phonon modes of hexagonal ZnO [27, 28, and 30]. The 528 cm^{-1} peak was attributed to the lattice defects or distortions that are usually found in Mn doped ZnO nanoparticles. The peak around 581 cm^{-1}due to ZnO (A_1(LO)) mode. The peak shifted to lower wavelength 571 cm^{-1} due to the formation Mn doping ZnO [29]. The Raman peaks at about 329 and 1068 cm^{-1} might be due to the $3E_{2H}$ - E_{2L} and A_1(TO) + E_1(TO) + E_{2L} multi phonon scattering modes, respectively [30].The sharpest and strongest peak is observed at about 437 cm^{-1}, which can be assigned to E_{2H} mode [31]. The mode 482 cm^{-1} is related to the vibration of oxygen atom in ZnO hexagonal wurtzite structure [32].

3.7. Differential scanning calorimetry

Differential scanning calorimetry carried out to identify the release of water and OH groups from Mn doped ZnO nanoparticles. Figure 7 showed that the temperature range from 25 to 500°C and an endothermic peak spreading from 80 to 160°C, this reveals that the materials liberate water molecules [23].The second endothermic peak from 190 to 275°C is due to the elimination of OH groups from the Mn_xZn_{1-x}Onanoparticles [33].

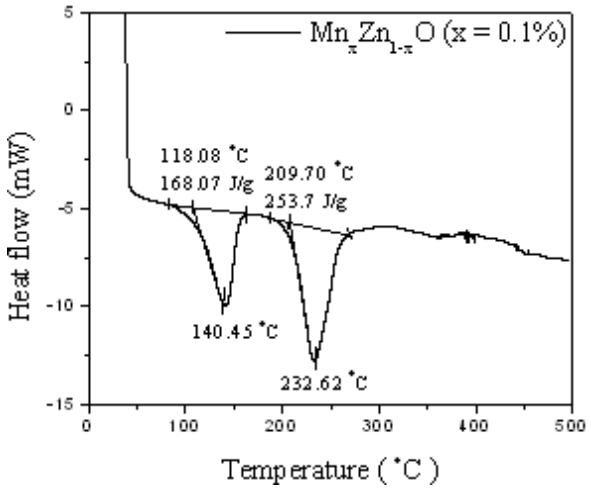

Fig 7: DSC analysis of $Mn_xZn_{1-x}O$ nanoparticles

3.8. UV-Visible spectroscopy

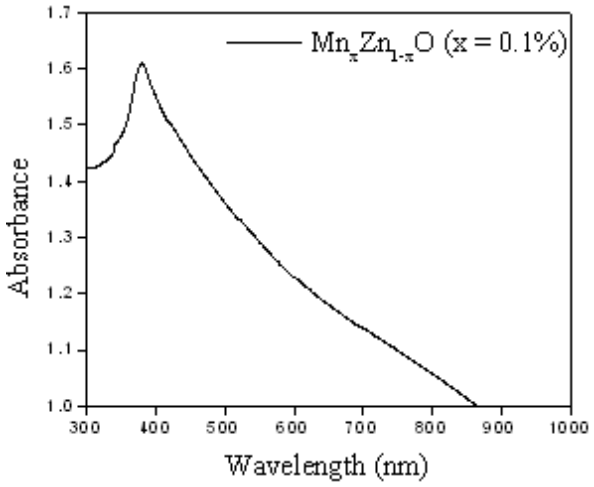

Fig 8: UV - Vis spectrum of $Mn_xZn_{1-x}O$ nanoparticles

The absorbance spectra of $Mn_xZn_{1-x}O$ (x = 0.1%) nanoparticles given in figure 8. This figure showed that the absorbance peak at 380 nm. The band gap energy of Mn doped ZnO nanoparticles could be determined using the following formula: E_{bg} =hc/ λ, where h is planck's constant (4.135667 x 10^{-15} eVs), c is the velocity of light (2.997924x10^8 m/s) and λ is the absorption wavelength in nm [1].

The band gap energy of undoped ZnO nanoparticles has comparatively high rather than band gap energy of doped ZnO (ie 1.9 eV).It may be due to the sp – d spin exchange interaction between the band electrons and localized d electrons of Mn ions substituting in cation sites [34]. Our experimental result indicates red shift in the band gap. This confirms the substitution of Mn in ZnO nanoparticles [35].

4. Antibacterial activity

The antibacterial activity of Mn doped ZnO nanoparticles (Sample) along with antibiotics are investigated against pathogenic bacteria such as *Escherichia coli* and *Staphylococcus aureus* using agar disc diffusion method. The diameter of inhibition zones around each disc is shown in figure 9 and the results are tabulated in Table 1.The results showed that, the toxicity of the sample increases with increase in concentration. Though the sample possesses activity, it could not reach the effectiveness of the standard drugs ampicillin and erythromycin. But, the sample moderate increase in inhibition zones were against penicillin.

ISSN 2321-807X
Volume 12 Number12
Journal of Advances in chemistry

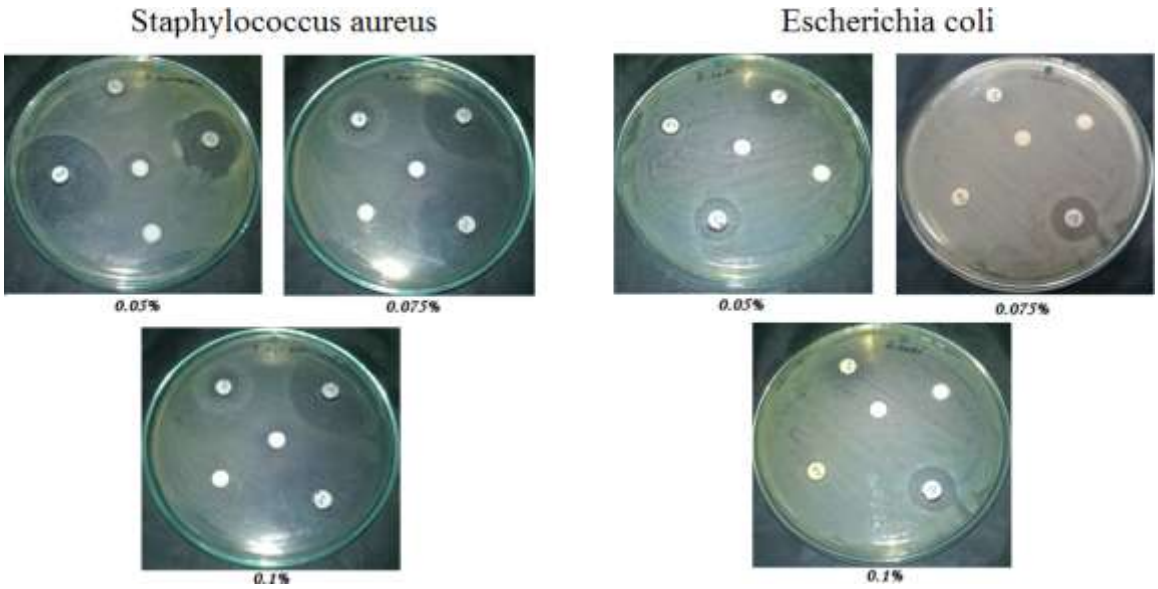

Fig 9: Antibacterial activities of $Mn_xZn_{1-x}O$ nanoparticles

Table-1: Zone of inhibition concentration of $Mn_xZn_{1-x}O$ (x=0.05, 0.075 and 0.1%) nanoparticles

S.No	Antibiotics	Diameter of inhibition Zone (mm)					
		Escherichia coli			Staphylococcus aureus		
		0.05	0.075	0.1	0.05	0.075	0.1
1	$Mn_xZn_{1-x}O$	8	9	10	14	16	36
2	Penicillin (P 10)	8	7	8	14	15	38
3	Ampicillin (A 10)	17	17	17	26	38	39
4	Erythromycin (E 15)	22	22	22	38	36	41

5. Conclusion

The Mn doped ZnO nanoparticles have been prepared by precipitation method. The prepared nanoparticles are annealed at 450°C and characterized on the basis of XRD, SEM, HRTEM, DSC and spectral (FT-IR, Electronic, Raman and EDX) data. Also, examined their antibacterial activities and found significant antibacterial activity.

6. References

[1] Tan, T. L., Lai, C.W., and S. B. A. Hamid, S.B.A. 2014. J. Nanomater. 2014, 1.

[2] Rekha, K., Nirmala, M., Manjula, G.N., and Anukaliani, A. 2010. Physica B. 405, 3180.

[3] Wang, J., Uma, S., and Klabunde, K.J. 2004. Appl. Catal. B: Environ. 48,151.

[4] Klosek, S., and Raftery, D. 2001. J. Phys. Chem. B. 105, 2815.

[5] Yin, X., Que, W., Liao, Y., Xie, H., and Fei, D. 2012. Surf. A: Physicochem. Eng. Asp. 410, 53.

[6] Mahmood, M.A., Baruah, S., and Dutta, J. 2011. Mater. Chem. Phys. 130, 531.

[7] Jayanthi Sharda, K., and Chawla, S. 2010. Appl. Surf. Sci. 256, 2630.

[8] Krohns, S., Lunkenheimer, P., Meissner, S., Reller, A., Gleich, B., Rathgeber, A., Gaugler, T., Buhl, H.U., Sinclair, D.C., and Loidl, A. 2011. Nat. Mater. 10, 899.

[9] Labuayai, S., Promarak, V., and Maensiri, S. 2009. Appl. Phys.A. 94, 755.

[10] Maensiri, S., Masingboon, C., Promarak, V., and Seraphin, S. 2007. Opt. Mat. 29, 1700.

[11] Ronning, C., Gao, P.X., Ding, Y., and Wang, Z.L. 2004. Appl. Phys. Lett. 84, 783.

[12] Prabhakar, R.R., Mathews, N., Jinesh, K.B., Karthik, K.R.G., Pramana, S.S., Varghese, B., Sow, C.H., and Mhaisalkar, S. 2012. J. Mater. Chem. 22, 9678.

[13] Elangovan, S.V., Sivakumar, N., and Chandramohan, V. J Mater Sci: Mater Electron, DOI 10.1007/s10854-015-3553-7.

[14] Ali, A.G., Dejenel,F.B., and Swart, H.C. 2012. Cent. Eur. J. Phys. 10, 478.

[15] Zhao, M., Wang, X., Ning, L., He, H., Jia, J., Zhang, L., and Li, X. 2010. J. Alloys Compd. 507, 97.

[16] Liu, Y., Xue, X., Yan, Z., Shi, J., Sun, L., and Wu, Y. 2014. Mater. Res. 17, 1658.

[17] Voicu,G., Oprea, O., Vasile, B.S., and Andronescu, E. 2013. DJNB. 8, 667.

[18] Ullah, R., and Dutta, J. 2008. J. Hazard. Mater. 156, 194.

[19] Vijayaprasath, G., Murugan, R., Shankaranarayanan, J., Dharuman, V., Ravi, G., and Hayakawa, Y. J. Mater. Sci: Mater Electron DOI 10-1007/s10854-015-3011-6.

[20] Husian, S., Alkhtaby, L.A., Giorgetti, E., Zoppi, A., and Miranda, M.M. 2014. J. Lumin. 145, 132.

[21] Alaria, J., Turek, P., Bernard, M., Bouloudenine, M., Berbadj, A., Brihi, N., Schmerber, G., Colis, S., and Dinia, A. 2005. Chem. Phys. Lett. 415, 337.

[22] Wang, Y., Liu, J., Liu, L., and Sun, D.D. 2012. J. Nanosci. Nanotechnol. 12, 1.

[23] Shafique, M.A., Shah, S.A., Nafees, M., Rasheed, K., and Ahmad, R. 2012. Int. Nano. Lett. 2, 31.

[24] Menon, A.S., Nandakumar, K., and Thomas, S. 2013. J. Nanosci. 1, 16.

[25] Ravichandrika, K., Kiranmayi, P., and Ravikumar, RVSSN. 2012. Int. J. Pharm. Pharm. Sci. 4, 336.

[26] Shi, Q., Zhang, J., Zhang, D., Wang, C., Yang, B., Zhang, B., and Wang, W. 2012. Mater. Sci. Eng. B.177, 689.

[27] Nghia, N.V., Trung, T.N., Truong, N. N. K., and Thuy, D.M. 2012. J. Synthesis Theory Appl. 1, 18.

[28] Sankara Reddy, B., Venkatramana Reddy, S., Koteeswara Reddy, N., and Prabhakara Reddy, Y. 2014. Adv. Mat. Lett. 5, 199.

[29] Toloman, D., Mesaros, A., Popa, A., Raita, O., Silipas, T.D., Vasile, B.S., Pana, O., and Giurgiu, L.M. 2013. J. Alloys Compd. 551, 502.

[30] Silambarasan, M., Saravanan, S., and Soga, T. 2014. e- J. Surf. Sci. Nanotech. 12, 283.

[31] Ma, C., Zhou, Z., Wei, H., Yang, Z., Wang, Z., and Zhang, Y. 2011. Nanoscale Res.Lett. 536, 6.

[32] Vijayaprasath, G., Ravi, G., Manikandan, M.R., Arivanandan, M., Navaneethan, M., and Hayakawa, Y. 2013. Asian J.Chem. 25, 0000.

[33] Tudor, I.A., Petriceanu, M., Piticescu, R.R., Piticescu, R.M., and Predescu, C. 2014. U.P.B. Sci. Bull., Series B.76, 207.

[34] Abdollahi, Y., Abdullah, A.H., Zainal, Z., and Yusof, N.A. 2011. IJBAS - IJENS.11, 44.

[35] Mote, V.D., Dargad, J.S., and Dole, B.N. 2013, Nanosci.Nanoengin.1, 116.